Threshold Resolvent Singularities and the Infrared Structure of Linearized Gravity

Michael Wilson

February 2026

Abstract

We identify a sharp geometric threshold governing the infrared spectral behavior of the spatial Lichnerowicz operator on asymptotically flat three–dimensional manifolds. When the Riemann curvature decays faster than r^{-3}, the operator remains spectrally short–range and exhibits regular low–energy scattering. At the inverse–cube decay rate $|\mathrm{Riem}(x)| \sim r^{-3}$, dispersion and curvature balance precisely: zero enters the essential spectrum and the weighted resolvent develops a quantitative threshold singularity,

$$\|\langle r\rangle^{-s}(L - i\varepsilon)^{-1}\langle r\rangle^{-s}\| \gtrsim \varepsilon^{-(1-s)}, \qquad s \in (1/2, 1).$$

The threshold limiting absorption principle therefore fails at zero energy.

This resolvent singularity provides a spatial mechanism underlying the infrared sector of linearized gravity. The same inverse–cube scaling governs the persistence of large–distance correlations, the irregularity of low–frequency scattering, and the emergence of soft gravitational modes. Numerical simulations of both a radial model and the full three–dimensional tensor operator confirm that $p = 3$ marks a sharp transition between spectrally negligible and marginal curvature. The same resolvent non-analyticity determines the late-time power-law relaxation of perturbations, establishing the tail exponent $t^{-(2\ell+3)}$ as a universal consequence of nonzero ADM mass.

More generally, in d spatial dimensions the critical decay $|\mathrm{Riem}(x)| \sim r^{-d}$ constitutes a universal boundary for curvature–coupled Laplace–type operators. The infrared structure of gravity is thus encoded directly in the spectral geometry of a Cauchy slice.

1 Introduction

The infrared structure of gravity governs the correlations that persist after gravitational radiation has passed. Effects such as gravitational memory, power-law tails, and soft graviton modes all originate from the long-range behavior of the field at large distances and low frequencies. These phenomena are usually formulated dynamically, in terms of radiation propagating to null infinity and the asymptotic symmetry structure of spacetime. Less clear, however, is how this infrared behavior is encoded directly on a spatial Cauchy slice.

The present work identifies a geometric threshold on an asymptotically flat spatial slice that determines whether linearized gravitational perturbations behave as purely radiative modes or develop an infrared sector. The key quantity is the rate at which background curvature decays at large radius. We show that in three spatial dimensions the inverse-cube decay

$$|\mathrm{Riem}(x)| \sim r^{-3}$$

marks the precise boundary between two qualitatively distinct regimes.

On one side of this boundary, when curvature decays faster than r^{-3}, the spatial Lichnerowicz operator governing stationary perturbations is spectrally indistinguishable from the flat tensor Laplacian. All finite-energy tensor excitations disperse, and the spectrum remains purely continuous and radiative.

At the critical inverse-cube rate, dispersion and curvature balance exactly. The operator then admits spatially extended, zero-energy configurations that are finite in norm yet nonlocal in extent. These marginal tensor modes define a continuous infrared sector touching zero energy without forming bound states. They represent the stationary precursors of the soft and memory phenomena familiar from the dynamical theory.

The same scaling reappears in a complementary radial model,

$$L_p = -\frac{d^2}{dr^2} + \frac{\ell(\ell+1)}{r^2} + \frac{C}{r^p},$$

which isolates the asymptotic competition between dispersion and curvature. Both analytic scaling arguments and numerical eigenvalue computations show that $p = 3$ is the unique marginal exponent in three dimensions. For $p > 3$, curvature becomes spectrally negligible; for $p < 3$, it acts as a

genuinely long-range potential. The transition at $p = 3$ is continuous but sharp, separating spectrally transparent geometries from those supporting marginal infrared structure.

More generally, in d spatial dimensions the same reasoning yields a universal relation

$$p_{\mathrm{crit}} = d,$$

expressing a dimensional balance between kinetic dispersion and curvature coupling. The inverse-cube decay in three dimensions is therefore not accidental but reflects a general geometric law: curvature decaying as r^{-d} marks the onset of infrared sensitivity for Laplace-type operators on asymptotically flat space.

This perspective reframes the infrared problem in gravity. Instead of deriving the soft sector from null infinity, asymptotic symmetries, or scattering amplitudes, we identify its origin in the spectral structure of the spatial Lichnerowicz operator itself. The appearance of zero-frequency, spatially extended tensor modes is thus a geometric phenomenon on a Cauchy slice, independent of S-matrix constructions or boundary symmetry arguments. In this way, the infrared structure of gravity emerges directly from the asymptotic scaling of curvature on a spatial hypersurface.

The paper proceeds as follows. Section 2 establishes the analytic and geometric framework for the spatial Lichnerowicz operator on asymptotically flat manifolds. Section 3 demonstrates that inverse-cube curvature decay produces marginal, spatially extended tensor modes and brings zero into the continuous spectrum. Section 4 generalizes the scaling argument to arbitrary dimension and identifies the universal threshold $p_{\mathrm{crit}} = d$. Section 5 provides numerical confirmation of the predicted scaling through both Rayleigh-quotient analysis and three-dimensional eigenvalue computations. Section 6 derives the soft graviton expansion directly from the outgoing spatial resolvent, recovering the Weinberg leading factor, identifying the subleading angular momentum term, and isolating the non-analytic threshold correction associated with inverse–cube curvature decay. Section 7 situates the result within existing work on spectral theory and long-range potentials.

2 Geometric Framework and Structural Parallels

To identify the geometric origin of infrared structure in linearized gravity, we begin with the operator that governs stationary tensor perturbations on a spatial slice. The analysis does not require the full time-dependent Einstein equations; rather, it hinges on the spectral properties of a Laplace-type operator determined by the background geometry.

Linearized gravity on an asymptotically flat slice

Let (Σ, g) be a smooth, asymptotically flat three-dimensional Riemannian manifold representing a time-symmetric slice of a vacuum spacetime. On the asymptotic end we assume

$$g_{ij} = \delta_{ij} + O(r^{-1}), \qquad \partial g_{ij} = O(r^{-2}), \qquad \partial^2 g_{ij} = O(r^{-3}),$$

so that the Riemann curvature decays as

$$|\mathrm{Riem}(x)| = O(r^{-3}).$$

Expanding the Einstein-Hilbert action to quadratic order in a perturbation $h_{\mu\nu}$ and imposing harmonic gauge yields a spatial quadratic form of the schematic type

$$\langle h, Lh \rangle,$$

where the spatial Lichnerowicz operator is

$$Lh = \nabla^* \nabla h + V_R h, \qquad (V_R h)_{ij} = -R^k{}_{ij}{}^\ell h_{k\ell}.$$

The first term represents kinetic dispersion, while the second encodes coupling to background curvature. The infrared behavior of the gravitational field is therefore controlled by how this curvature term behaves at large radius.

Curvature as an effective potential

At large distances, the Lichnerowicz operator has the universal Laplace-type structure

$$L \sim -\nabla^2 + V(r),$$

where $V(r)$ arises from curvature components and decays according to the asymptotic geometry. In three spatial dimensions, curvature generically falls off as r^{-3} for isolated vacuum solutions.

From the spectral point of view, curvature therefore acts as an effective potential. If it decays sufficiently fast, it becomes negligible in the far field and the operator behaves as in flat space. If it decays too slowly, it remains influential at arbitrarily large radius and alters the low-energy structure of the field.

The problem of gravitational infrared behavior thus reduces to a long-range versus short-range classification of curvature-induced potentials.

Structural parallel with gauge theory

This structure is not unique to gravity. For a Yang-Mills connection A, the covariant Laplacian acting on adjoint fields takes the form

$$\Delta_A = -\nabla^2 + \mathrm{ad}(F_A),$$

where the curvature F_A plays the same structural role as R_{ijkl} in the gravitational case. In both theories, the quadratic operator consists of a Laplacian plus a curvature-dependent potential.

Dimensional analysis then immediately suggests a common threshold. In three spatial dimensions, a potential of order r^{-3} is marginal: it decays just slowly enough to compete with dispersion over large volumes. Faster decay renders it spectrally negligible; slower decay produces genuinely long-range coupling.

Thus, before any detailed analysis, one expects the inverse-cube decay rate to mark a geometric boundary between radiative and infrared-sensitive behavior. The remainder of this work makes that expectation precise for the spin-2 sector.

3 Infrared Spectrum and Marginal Gravitational Modes

We now turn to the regime in which the background curvature decays at the inverse-cube rate,

$$|\mathrm{Riem}(x)| \sim r^{-3},$$

and show that this decay marks a sharp boundary in the infrared behavior of linearized gravity. At this rate, the spatial operator governing tensor perturbations admits zero-frequency configurations that remain spatially extended and finite in energy. These modes are neither localized bound states nor freely radiating waves, but sit precisely at the threshold between the two.

Throughout this section, we consider a smooth, asymptotically flat spatial slice (Σ, g) with a single asymptotic end, satisfying

$$g_{ij} = \delta_{ij} + O(r^{-1}), \qquad \partial g_{ij} = O(r^{-2}), \qquad \partial^2 g_{ij} = O(r^{-3}),$$

so that the curvature decays as $|\mathrm{Riem}(x)| = O(r^{-3})$. On such a background, stationary perturbations of the vacuum Einstein equations in harmonic gauge are governed by the spatial Lichnerowicz operator

$$Lh = \nabla^*\nabla h + V_R h, \qquad (V_R h)_{ij} = -R^k{}_{ij}{}^\ell h_{k\ell},$$

acting on symmetric, trace-free tensor fields.

Physical degrees of freedom and gauge fixing

The physical content of linearized gravity resides in transverse-traceless tensor modes. The harmonic gauge condition $\nabla^j h_{ij} = 0$ may be enforced by a standard elliptic gauge correction involving the vector Laplacian

$$\Delta_V = \nabla^*\nabla + \mathrm{Ric},$$

which is invertible on asymptotically flat slices under mild topological assumptions. This allows any approximate configuration to be corrected to a transverse one without changing its leading asymptotic behavior.

Once this gauge is imposed, the operator L becomes self-adjoint on $L^2(\Sigma)$, and its spectrum determines the infrared structure of the gravitational field. In particular, the presence or absence of zero energy in the spectrum controls whether arbitrarily low-frequency tensor excitations behave as freely radiating waves or develop long-range spatial correlations.

Scaling argument and asymptotic tensor modes

The inverse-cube decay rate emerges naturally from a simple scaling argument. At large radius, the kinetic term contributes derivatives of order r^{-2},

while the curvature coupling contributes an effective potential of order r^{-3}. Exactly at this rate, neither term dominates asymptotically.

To make this balance explicit, consider a family of transverse-traceless tensor configurations supported on spherical shells at large radius. Let $H_{ij}(\omega)$ be a trace-free, divergence-free tensor harmonic on the unit sphere, and define

$$h_n(r,\omega) = A_n\,\phi_n(r)\,r^{-1}H_{ij}(\omega),$$

where ϕ_n is a smooth cutoff localizing the field to an annulus of radius $r \sim n$. The normalization factor $A_n \sim n^{-1/2}$ ensures that each configuration has unit L^2 norm.

Physically, these configurations describe increasingly distant, increasingly spread-out tensor distortions whose angular structure is fixed while their radial support drifts to infinity. They represent candidate infrared modes of the gravitational field.

Acting on such fields, the flat Laplacian annihilates the leading r^{-1} behavior, while derivatives of the cutoff produce contributions suppressed by powers of n^{-1}. The curvature term contributes

$$V_R h_n \sim r^{-3} h_n,$$

which, after integration over the shell, also yields a contribution that vanishes as $n \to \infty$. As a result, the total action of the operator satisfies

$$\|Lh_n\|_{L^2} \longrightarrow 0 \qquad (n \to \infty),$$

even though each configuration remains normalized.

After enforcing the transverse gauge condition, this family becomes a sequence of physical tensor modes whose energy approaches zero while their spatial extent diverges. These are not localized bound states; rather, they are threshold configurations that live arbitrarily far out in the asymptotic region.

Emergence of an infrared continuum

The existence of such configurations has a direct spectral interpretation. Because these modes are normalized, escape to infinity, and are annihilated by the operator in the limit, zero energy belongs to the continuous part of the

spectrum. In physical terms, the gravitational field admits arbitrarily low-frequency tensor excitations that are not suppressed by curvature, even at infinite radius.

This phenomenon occurs only at the inverse-cube decay rate. For faster decay, the curvature coupling becomes negligible in the far field, and all finite-energy perturbations behave as freely radiating modes. For slower decay, curvature acts as a genuinely long-range potential and can strengthen infrared coupling further. The rate $|\mathrm{Riem}| \sim r^{-3}$ therefore marks the precise boundary between spectrally transparent and infrared-sensitive gravitational backgrounds.

Interpretation

The appearance of zero-energy, spatially extended tensor modes is the stationary signature of infrared physics in gravity. In the full time-dependent problem, these modes correspond to the $\omega \to 0$ limit of gravitational radiation and underlie familiar phenomena such as soft gravitons, power-law tails, and gravitational memory. The inverse-cube decay therefore identifies the geometric threshold at which linearized gravity ceases to be purely radiative and develops a continuous infrared sector.

Breakdown of the Limiting Absorption Principle and Threshold Resolvent Growth

The existence of marginal tensor configurations at inverse-cube curvature decay has a sharper analytic consequence: the weighted resolvent of the spatial Lichnerowicz operator develops a quantitative singularity at zero energy.

For Laplace-type operators on asymptotically flat manifolds, the limiting absorption principle (LAP) asserts that for suitable weights $s > 1/2$, the boundary values

$$(L - i\varepsilon)^{-1}$$

remain uniformly bounded between weighted L^2 spaces as $\varepsilon \to 0^+$. Physically, this corresponds to regular low-frequency scattering and the absence of threshold obstructions.

At the critical decay rate $|\mathrm{Riem}(x)| \sim r^{-3}$, this uniform bound fails. More precisely, define

$$T_\varepsilon = \langle r \rangle^{-s} (L - i\varepsilon)^{-1} \langle r \rangle^{-s}, \qquad s \in (1/2, 1).$$

Then there exists $c > 0$ such that for all sufficiently small $\varepsilon > 0$,

$$\|T_\varepsilon\|_{L^2 \to L^2} \;\geq\; c\,\varepsilon^{-(1-s)}.$$

In particular, the weighted resolvent norm diverges as $\varepsilon \to 0^+$, and the threshold limiting absorption principle fails.

The mechanism is directly tied to the Weyl sequence constructed in Section 3. For inverse-cube curvature decay one may construct transverse-traceless tensor fields $\tilde{h}_n$ supported on annuli of radius $r \sim n$ such that

$$\|\tilde{h}_n\|_{L^2} = 1, \qquad \|L\tilde{h}_n\|_{L^2} \lesssim n^{-2}.$$

On the support of $\tilde{h}_n$, one has $\langle r \rangle \sim n$, so

$$\|\langle r \rangle^{-s} \tilde{h}_n\|_{L^2} \sim n^{-s}, \qquad \|\langle r \rangle^{s} \tilde{h}_n\|_{L^2} \sim n^{s}.$$

Defining

$$g_{n,\varepsilon} = \langle r \rangle^s (L - i\varepsilon)\tilde{h}_n,$$

one obtains

$$\|g_{n,\varepsilon}\|_{L^2} \lesssim n^{s-2} + \varepsilon n^s.$$

Choosing $\varepsilon \sim n^{-2}$ gives

$$\|g_{n,\varepsilon}\|_{L^2} \lesssim n^{s-2}.$$

Since

$$T_\varepsilon g_{n,\varepsilon} = \langle r \rangle^{-s} \tilde{h}_n,$$

it follows that

$$\|T_\varepsilon\| \gtrsim \frac{n^{-s}}{n^{s-2}} = n^{2-2s}.$$

Setting $n = \varepsilon^{-1/2}$ yields

$$\|T_\varepsilon\| \gtrsim \varepsilon^{-(1-s)}.$$

The characteristic scale $R \sim \varepsilon^{-1/2}$ identifies the spatial radius at which dispersion (R^{-2}) balances the spectral parameter ε. The configurations obstructing the resolvent are therefore increasingly remote, spatially extended tensor distortions whose support drifts to infinity as $\varepsilon \to 0$.

This scaling is precisely the geometric origin of infrared persistence. The modes responsible for the resolvent singularity are the same extended configurations that carry memory-type information at large distances. As $\varepsilon \to 0$,

the obstruction migrates outward rather than localizing, reflecting the fact that low-frequency gravitational data is stored in correlations at arbitrarily large radius.

Thus the inverse-cube curvature decay produces a genuine *threshold singularity of the resolvent*. The operator does not admit uniform low-energy scattering behavior, and the soft sector of linearized gravity emerges directly from this breakdown of threshold resolvent regularity.

4 Dimensional Scaling and the Infrared Phase Structure of Gravity

The inverse-cube decay identified in the previous section reflects a general balance between dispersion and curvature coupling that depends only on spatial dimension. In d spatial dimensions, curvature decaying as r^{-d} marks the boundary between radiative and infrared-sensitive behavior.

Dimensional balance between dispersion and curvature

Consider a linearized field on an asymptotically flat spatial slice Σ_d of dimension d. The quadratic operator governing stationary perturbations has the schematic form

$$L_d \sim -\nabla^2 + V(r),$$

where the Laplacian represents dispersion and $V(r)$ is a curvature-induced potential with asymptotic decay

$$V(r) \sim r^{-p}.$$

The infrared behavior is determined by which of these two effects dominates asymptotically. If curvature decays sufficiently fast, it becomes irrelevant at large distances. If it decays too slowly, curvature continues to influence the field arbitrarily far out.

Scaling of extended modes

To see this balance explicitly, consider normalized configurations supported on shells of radius R. For such configurations, the Laplacian contributes

energy of order R^{-2}, while the curvature term contributes

$$\Delta E_V(R) \sim \int_R^{2R} r^{-p} |h(r)|^2 r^{d-1} dr.$$

For physically relevant tensor modes in an asymptotically flat geometry, the amplitude scales as

$$|h(r)| \sim r^{-(d-2)/2},$$

which is not a choice but follows from the asymptotic flatness falloff conditions together with finite L^2 energy on the spatial slice. Substituting this behavior yields

$$\Delta E_V(R) \sim \int_R^{2R} r^{d-1-p-(d-2)} dr = \int_R^{2R} r^{1-p} dr.$$

This integral vanishes as $R \to \infty$ when $p > d$, but remains of order one when $p = d$. At exactly this rate, curvature competes with dispersion at all scales. Thus the critical decay rate is

$$p_{\text{crit}} = d.$$

Infrared phases across dimensions

Three regimes follow immediately.

If curvature decays faster than r^{-d}, extended modes behave as in flat space and the spectrum is purely radiative.

At the critical decay rate r^{-d}, curvature and dispersion balance. The operator admits marginal, spatially extended configurations whose energy approaches zero but never localizes. These modes define a continuous infrared sector touching zero energy without forming bound states.

If curvature decays more slowly than r^{-d}, it acts as a genuinely long-range potential and enhances infrared coupling.

Universality

The relation

$$p_{\text{crit}} = d$$

is not specific to gravity. The same scaling governs gauge fields, where curvature enters as an effective potential of identical dimensional weight. In all

such cases, the long-range structure of the field is controlled by geometry: curvature decaying as r^{-d} marks the onset of infrared sensitivity.

In three dimensions this reduces to the inverse-cube decay r^{-3}, explaining why that rate plays a distinguished role in gravitational infrared physics.

5 Numerical Verification of the Spectral Threshold

The analytic arguments of Sections 3–4 predict that the spectral transition occurs at $p = 3$: curvature decaying faster than r^{-3} becomes spectrally negligible, while the inverse–cube decay marks the onset of marginal long–range coupling. We now test this prediction through two independent numerical diagnostics:

(i) a Rayleigh–quotient scaling analysis of an asymptotic radial model, and (ii) a computation of the lowest eigenvalues of the full three–dimensional tensor operator.

Both diagnostics probe the same question: does the infrared spectral behavior change sharply at $p = 3$?

The spatial operator is discretized on a finite Cartesian domain $\Omega = [-R_{\max}, R_{\max}]^3$ with Dirichlet boundaries. Transverse–traceless constraints are enforced by a penalty method, and convergence is verified by grid refinement and parameter sweeps. A detailed description of the discretization, penalty functional, solver implementation, and stability tests is provided in Appendix D. Here we focus only on the spectral results.

5.1 Rayleigh–Quotient Scaling

The analytic scaling argument predicts that for the radial model

$$L_p = -\frac{d^2}{dr^2} + \frac{\ell(\ell+1)}{r^2} + \frac{C}{r^p},$$

the energy shift produced by the curvature term behaves as

$$\Delta E(R, p) \sim R^{-(p-2)}.$$

To test this prediction, we evaluate the Rayleigh quotient

$$E[\phi] = \frac{\int_R^{2R} \big(|\phi'(r)|^2 + V_p(r)|\phi(r)|^2\big) r^2 dr}{\int_R^{2R} |\phi(r)|^2 r^2 dr},$$

with a normalized bump function ϕ supported on $[R, 2R]$. The flat case $C = 0$ defines the reference energy E_{free}, and we measure $\Delta E(R, p) = E - E_{\text{free}}$.

Table 1 lists the results. The fitted slopes $\alpha(p) \approx -(p-2)$ confirm the analytic scaling.

Table 1: Rayleigh-quotient energy shift $\Delta E(R, p)$ for $C = -1$. The power-law scaling with R follows $\Delta E \sim R^{-(p-2)}$, confirming that $p = 3$ behaves as the marginal case separating decaying from saturating behavior.

p	R	$\Delta E(R,p)$	E_{full}	E_{free}
2.00	10	-2.85×10^{-2}	1.50×10^{-1}	1.54×10^{-1}
	20	-2.85×10^{-2}	3.74×10^{-2}	3.85×10^{-2}
	40	-2.85×10^{-2}	9.36×10^{-3}	9.63×10^{-3}
	80	-2.85×10^{-2}	2.34×10^{-3}	2.41×10^{-3}
	160	-2.85×10^{-2}	5.85×10^{-4}	6.02×10^{-4}
	320	-2.85×10^{-2}	1.46×10^{-4}	1.50×10^{-4}
	640	-2.85×10^{-2}	3.65×10^{-5}	3.76×10^{-5}
2.50	10	-7.39×10^{-3}	1.53×10^{-1}	1.54×10^{-1}
	20	-5.23×10^{-3}	3.83×10^{-2}	3.85×10^{-2}
	40	-3.69×10^{-3}	9.59×10^{-3}	9.63×10^{-3}
	80	-2.61×10^{-3}	2.40×10^{-3}	2.41×10^{-3}
	160	-1.85×10^{-3}	6.01×10^{-4}	6.02×10^{-4}
	320	-1.31×10^{-3}	1.50×10^{-4}	1.50×10^{-4}
	640	-9.23×10^{-4}	3.76×10^{-5}	3.76×10^{-5}
3.00	10	-1.92×10^{-3}	1.54×10^{-1}	1.54×10^{-1}
	20	-9.62×10^{-4}	3.85×10^{-2}	3.85×10^{-2}
	40	-4.81×10^{-4}	9.63×10^{-3}	9.63×10^{-3}
	80	-2.40×10^{-4}	2.41×10^{-3}	2.41×10^{-3}
	160	-1.20×10^{-4}	6.02×10^{-4}	6.02×10^{-4}
	320	-6.01×10^{-5}	1.50×10^{-4}	1.50×10^{-4}
	640	-3.01×10^{-5}	3.76×10^{-5}	3.76×10^{-5}
3.50	10	-5.02×10^{-4}	1.54×10^{-1}	1.54×10^{-1}
	20	-1.78×10^{-4}	3.85×10^{-2}	3.85×10^{-2}
	40	-6.28×10^{-5}	9.63×10^{-3}	9.63×10^{-3}
	80	-2.22×10^{-5}	2.41×10^{-3}	2.41×10^{-3}
	160	-7.85×10^{-6}	6.02×10^{-4}	6.02×10^{-4}

Continued on next page

Table 1: Rayleigh-quotient energy shift $\Delta E(R,p)$ (continued).

p	R	$\Delta E(R,p)$	E_{full}	E_{free}
	320	-2.78×10^{-6}	1.50×10^{-4}	1.50×10^{-4}
	640	-9.81×10^{-7}	3.76×10^{-5}	3.76×10^{-5}
4.00	10	-1.32×10^{-4}	1.54×10^{-1}	1.54×10^{-1}
	20	-3.29×10^{-5}	3.85×10^{-2}	3.85×10^{-2}
	40	-8.23×10^{-6}	9.63×10^{-3}	9.63×10^{-3}
	80	-2.06×10^{-6}	2.41×10^{-3}	2.41×10^{-3}
	160	-5.14×10^{-7}	6.02×10^{-4}	6.02×10^{-4}
	320	-1.29×10^{-7}	1.50×10^{-4}	1.50×10^{-4}
	640	-3.21×10^{-8}	3.76×10^{-5}	3.76×10^{-5}

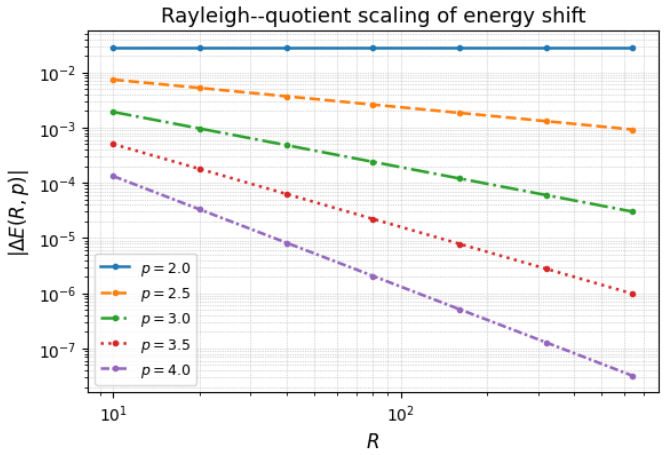

Figure 1: Log–log scaling of $|\Delta E(R,p)|$. Measured slopes $\alpha(p) \approx -(p-2)$ agree with the analytic prediction. The case $p = 3$ produces the marginal scaling $\Delta E \sim R^{-1}$.

5.2 Three–Dimensional Eigenvalue Convergence

We next compute the lowest eigenvalue λ_1 of the discretized tensor operator for several decay exponents p and increasing domain size $R_{\max}$. If curvature is spectrally negligible, $\lambda_1(R_{\max})$ should scale as $R_{\max}^{-2}$, reflecting approach to the continuum threshold.

Table 2: Lowest eigenvalue λ_1 of the discretized tensor operator for several decay exponents p and outer radii $R_{\max}$. Decreasing λ_1 with larger $R_{\max}$ confirms convergence toward the infinite-volume limit.

p	$R_{\max}$	λ_1
flat	6	0.2044
	10	0.0739
	14	0.0377
	18	0.0228
	20	0.0185
2.0	6	0.1466
	10	0.0435
	14	0.0192
	18	0.0102
	20	0.0078
2.5	6	0.1828
	10	0.0651
	14	0.0334
	18	0.0203
	20	0.0166
3.0	6	0.1965
	10	0.0711
	14	0.0365
	18	0.0222
	20	0.0180
3.5	6	0.2016
	10	0.0730
	14	0.0374
	18	0.0227
	20	0.0184
4.0	6	0.2035
	10	0.0736
	14	0.0376
	18	0.0228
	20	0.0185

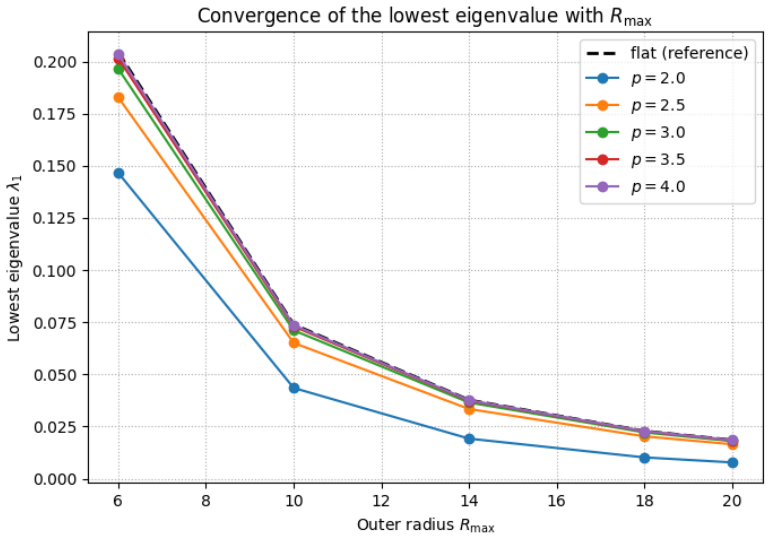

Figure 2: Convergence of λ_1 with domain size $R_{\max}$. For $p \geq 3$, eigenvalues approach the flat–space scaling $\lambda_1 \sim R_{\max}^{-2}$. For $p < 3$, curvature produces a progressively stronger infrared shift.

For $p \geq 3$, the lowest eigenvalue scales as $\lambda_1(R_{\max}) \sim R_{\max}^{-2}$, consistent with approach to the continuum threshold and the absence of bound states. For $p < 3$, the slower decay of curvature enhances the infrared coupling and lowers λ_1, but no discrete negative modes appear. The transition is continuous rather than confining.

Both numerical diagnostics reproduce the analytic prediction: the spectral transition occurs at $p = 3$. For faster curvature decay, the spectrum is indistinguishable from flat space. At the inverse–cube rate, curvature remains spectrally relevant at all scales, producing marginal behavior without discrete confinement. The numerical results therefore confirm that $p = 3$ constitutes a sharp infrared threshold for the spatial Lichnerowicz operator.

6 Soft Graviton Structure from the Spatial Resolvent

We now reorganize the infrared structure of linearized gravity around a single spatial object: the outgoing resolvent of the transverse-traceless (TT) Lich-

nerowicz operator on a Cauchy slice. The soft limit is therefore a threshold problem for an elliptic operator. Three conclusions emerge.

First, the leading $1/\omega$ soft graviton pole is purely kinematic. It originates in the Fourier transform of asymptotically inertial sources and is independent of the background curvature decay rate. Second, ordinary geometric corrections enter at $O(\omega^0)$ and reproduce the known subleading soft factor (for spinless external particles) together with background-dependent propagation effects. Third, at the inverse-cube curvature threshold $|\mathrm{Riem}| \sim r^{-3}$, the outgoing resolvent becomes non-analytic at $\omega = 0$; this produces an additional threshold correction to the soft expansion whose existence is forced by the failure of the limiting absorption principle (LAP). Finally, the static limit of the resolvent encodes gravitational memory directly through the spatial Green operator.

6.1 The spatial operator, TT sector, and outgoing resolvent

Let (Σ, g) be a three-dimensional asymptotically Euclidean slice with

$$g_{ij} = \delta_{ij} + O(r^{-1}), \qquad \partial g_{ij} = O(r^{-2}), \qquad \partial^2 g_{ij} = O(r^{-3}),$$

so that in the critical case $|\mathrm{Riem}(x)| \sim C\, r^{-3}$ as $r \to \infty$. The spatial Lichnerowicz operator acting on symmetric two-tensors is

$$L = \nabla^*\nabla + V_R, \qquad (V_R h)_{ij} = -R_{i\ell jm}\, h^{\ell m}.$$

The physical degrees of freedom of linearized gravity lie in the TT sector. The TT projection is defined elliptically. Given a symmetric two-tensor h, one solves

$$\Delta_V X = \nabla \cdot h, \qquad \Delta_V = \nabla^*\nabla + \mathrm{Ric},$$

and removes the pure-gauge and trace parts:

$$\Pi^{\mathrm{TT}} h = h - \mathcal{L}_X g - \tfrac{1}{3}(\mathrm{tr}\, h)\, g.$$

This projection is nonlocal but purely elliptic in the spatial variables; for compactly supported scattering sources it does not introduce new frequency singularities in the soft limit.

Let $\mathcal{J}^{\mathrm{TT}}$ denote the already TT-projected forcing term. The linearized wave equation is

$$(\partial_t^2 + L)\, h(t,x) = \mathcal{J}^{\mathrm{TT}}(t,x), \qquad h(t,x) = 0 \text{ for } t \ll 0.$$

With the Fourier convention

$$\widehat{h}(\omega,x) = \int_{\mathbb{R}} e^{i\omega t} h(t,x)\, dt, \qquad h(t,x) = \frac{1}{2\pi}\int_{\mathbb{R}} e^{-i\omega t}\widehat{h}(\omega,x)\, d\omega,$$

the frequency-domain equation becomes

$$(L - \omega^2)\,\widehat{h}(\omega,x) = \widehat{\mathcal{J}}^{\mathrm{TT}}(\omega,x).$$

The retarded solution is obtained by the outgoing boundary value

$$\widehat{h}_{\mathrm{ret}}(\omega) = R_{\mathrm{out}}(\omega)\,\widehat{\mathcal{J}}^{\mathrm{TT}}(\omega), \qquad R_{\mathrm{out}}(\omega) = \big(L - (\omega + i0)^2\big)^{-1}.$$

Thus the soft limit $\omega \to 0$ is governed by the threshold behavior of $R_{\mathrm{out}}(\omega)$ in the TT sector.

6.2 Threshold behavior of the resolvent

When curvature decays faster than r^{-3}, the curvature coupling is spectrally short-range. The LAP holds at zero energy: for $s > 1/2$ the weighted boundary values

$$\langle r\rangle^{-s} R_{\mathrm{out}}(\omega) \langle r\rangle^{-s}$$

extend continuously to $\omega = 0$ as bounded operators on $L^2(\Sigma)$. In this regime the resolvent admits an analytic expansion at low frequency in weighted spaces.

At the inverse-cube decay rate $|\mathrm{Riem}| \sim r^{-3}$, the LAP fails. The theorem of Section 3 yields, for $s \in (1/2, 1)$,

$$\big\| \langle r\rangle^{-s} R_{\mathrm{out}}(\omega) \langle r\rangle^{-s} \big\| \gtrsim \omega^{-2(1-s)} \qquad \text{as } \omega \to 0^+. \tag{1}$$

This growth rules out a Taylor expansion of $R_{\mathrm{out}}(\omega)$ at $\omega = 0$ in weighted spaces. The obstruction is carried by TT configurations localized on annuli whose radius diverges as $\omega \to 0$, as exhibited by the Weyl sequence construction in Appendix E.

Motivated by the borderline threshold expansions of three-dimensional Schrödinger operators (Jensen-Kato and subsequent refinements), we write the low-frequency structure in the form

$$R_{\text{out}}(\omega; x, y) = G(x, y) + i\omega\, H_1(x, y) + \omega^2\, \Phi(\omega)\, H_2(x, y) + O(\omega^2), \tag{2}$$

where $G = L^{-1}$ is the static Green operator, H_1 is bounded in weighted spaces, and $\Phi(\omega)$ is a real threshold function that is non-analytic at $\omega = 0$. In the short-range case $p > 3$, $\Phi(\omega) \equiv 1$ and the expansion is analytic. At $p = 3$, the LAP failure forces $\Phi(\omega) \to \infty$ as $\omega \to 0^+$. In the scalar borderline theory $\Phi(\omega) \sim \log \omega$, and the same logarithmic behavior is expected here; we will use only the structural fact that a non-analytic threshold contribution is present.

6.3 Radiation zone asymptotics and the leading soft pole

On $\mathbb{R}^3$ the free outgoing kernel is

$$G_0(\omega; x, y) = \frac{e^{i\omega|x-y|}}{4\pi|x-y|}.$$

In the radiation zone, with $r = |x| \to \infty$ and y in a compact region,

$$G_0(\omega; x, y) = \frac{e^{i\omega r}}{4\pi r} e^{-i\omega\hat{q}\cdot y} + O(r^{-2}), \qquad \hat{q} = \frac{x}{r}.$$

For asymptotically flat (Σ, g) the full TT resolvent has the same leading structure,

$$R^{\text{TT}}_{\text{out}}(\omega; x, y) = \frac{e^{i\omega r}}{4\pi r}\, \mathcal{K}(\omega, \hat{q}; y) + O(r^{-2}), \tag{3}$$

where $R^{\text{TT}}_{\text{out}}$ denotes the resolvent restricted to the TT sector acting on already TT-projected sources. No additional source-side projection appears in $\mathcal{K}$.

Consider a compact scattering event involving particles with asymptotic four-momenta p^μ_n. The Fourier transform of the stress-energy has the kinematic pole

$$\widehat{T}^{\mu\nu}(\omega, y) \sim \sum_n \frac{p^\mu_n p^\nu_n}{m_n} \frac{i}{\omega - \vec{q}\cdot\vec{v}_n + i0} + \text{regular}, \qquad \vec{q} = \omega\hat{q}. \tag{4}$$

After solving the elliptic constraints and projecting onto the TT sector, one obtains

$$\widehat{\mathcal{J}}^{\mathrm{TT}}(\omega, y) = \frac{1}{\omega}\,\mathcal{S}(y) + \mathcal{R}(\omega, y), \tag{5}$$

where $\mathcal{R}$ is regular at $\omega = 0$ and $\mathcal{S}(y)$ is chosen to be real; the explicit factor of i in (4) is absorbed into its definition. Because the source is compactly supported, the elliptic inversion samples only short-distance behavior of the Green operators and is insensitive to the large-radius threshold structure.

Combining (3) and (5), the radiative amplitude satisfies

$$\mathcal{A}(\omega, \hat{q}) = \frac{1}{\omega}\Pi^{\mathrm{TT}}(\hat{q}) \int_{\Sigma} \mathcal{S}(y)\, dV_g(y) + O(\omega^0). \tag{6}$$

The $1/\omega$ pole is therefore purely kinematic. Evaluating the integral yields Weinberg's soft factor

$$\mathcal{A}(\omega, \hat{q}) \underset{\omega\to 0}{\sim} \frac{1}{\omega} \sum_n \eta_n \frac{p_n^\mu p_n^\nu \varepsilon_{\mu\nu}(\hat{q})}{p_n \cdot q},$$

independent of the curvature decay rate.

6.4 Subleading soft structure and the threshold correction

The soft expansion has the schematic form

$$\mathcal{A}(\omega, \hat{q}) = \frac{1}{\omega} S^{(0)}(\hat{q}) + S^{(1)}(\hat{q}) + \omega\, \Phi(\omega)\, S^{(\mathrm{th})}(\hat{q}) + O(\omega). \tag{7}$$

Since $\Phi(\omega) \to \infty$ as $\omega \to 0^+$ in the critical case, the term $\omega\Phi(\omega)$ is parametrically larger than any analytic $O(\omega)$ correction, justifying its placement in (7).

The term $S^{(1)}$ receives contributions from the phase expansion $e^{-i\omega\hat{q}\cdot y}$ and from regular curvature corrections. The phase expansion produces the *orbital* angular momentum contribution

$$S^{(1)}(\hat{q}) = \sum_n \eta_n \frac{\varepsilon_{\mu\nu}(\hat{q}) p_n^\mu q_\rho J_{n,\mathrm{orb}}^{\rho\nu}}{p_n \cdot q}.$$

For spinless external particles this exhausts the subleading soft factor and matches the Cachazo-Strominger result. For spinning particles, additional

spin-dependent terms arise from the detailed tensorial source coupling rather than from the propagation phase.

The threshold correction arises from the non-analytic resolvent term in (2). It has the form

$$S^{(\mathrm{th})}(\hat{q}) = \Pi^{\mathrm{TT}}(\hat{q}) \int_{\Sigma} H_2(\hat{q}, y)\mathcal{S}(y)\, dV_g(y).$$

This term vanishes in the short-range regime and is intrinsically tied to LAP failure at the inverse-cube threshold.

6.5 Memory from the static resolvent

Memory is extracted by

$$\Delta h(x) = \lim_{\omega \to 0} i\omega\, \widehat{h}_{\mathrm{ret}}(\omega, x). \tag{8}$$

Using (5) and the resolvent expansion yields

$$\Delta h(x) = G * \mathcal{S}(x) = \int_{\Sigma} G(x, y)\mathcal{S}(y)\, dV_g(y), \qquad G = L^{-1}. \tag{9}$$

The resolvent growth bound (1) implies enhanced spectral weight near $\lambda = 0$. By the spectral theorem and a Tauberian argument, this enhancement transfers to the large-separation tail of $G(x, y)$, strengthening the spatial memory response in the critical case.

In the null-infinity framework, memory is expressed in terms of Bondi news. Equation (9) gives an equivalent Cauchy-slice representation. Verifying explicitly that the spatial Green's formulation reproduces the Bondi memory formula would provide a direct bridge between the resolvent-based picture and the asymptotic symmetry framework, and a detailed comparison is deferred to subsequent work.

Late-time tails from the threshold resolvent singularity

The non-analyticity of the outgoing resolvent at threshold has a direct dynamical consequence: it governs the late-time relaxation of linear perturbations on any asymptotically flat vacuum background with nonzero ADM mass.

Let $h(t,x)$ denote the retarded solution of the linearized equation with source J^{TT}. In frequency space one may write

$$h(t,x) = \frac{1}{2\pi}\int_{-\infty}^{\infty} e^{-i\omega t} R_{\mathrm{out}}(\omega)\, \widehat{J}^{\mathrm{TT}}(\omega,x)\, d\omega, \tag{10}$$

where $R_{\mathrm{out}}(\omega) = (L - \omega^2 - i0)^{-1}$ is the outgoing resolvent of the spatial Lichnerowicz operator.

As $t \to \infty$, the integral is determined by the lowest singularity of the integrand in ω. If the resolvent is analytic at $\omega = 0$, the inverse Fourier integral may be deformed into the lower half-plane and the late-time decay is exponential (or super-polynomial). If instead $\omega = 0$ is a branch point of the resolvent, the late-time behaviour is governed by the discontinuity across the associated branch cut and is necessarily of power-law type. Thus the existence of power-law tails is equivalent to a threshold non-analyticity of the resolvent.

Origin of the branch point in the critical case. In Section 3 it was shown that in three spatial dimensions the curvature coupling in the Lichnerowicz operator is critical when

$$|\mathrm{Riem}(x)| \sim C_M r^{-3}, \qquad r \to \infty, \tag{11}$$

with C_M proportional to the ADM mass M. We now identify the resulting small-frequency structure of the resolvent.

After separation into spherical harmonics, each angular momentum channel ℓ satisfies a radial equation of Schrödinger type

$$\left(-\partial_r^2 + \frac{\ell(\ell+1)}{r^2} + V(r)\right) u_\ell(r,k) = k^2 u_\ell(r,k), \qquad k = \omega, \tag{12}$$

where the effective potential satisfies

$$V(r) = \frac{C}{r^3} + O(r^{-4}), \qquad r \to \infty. \tag{13}$$

The outgoing Green function in this channel is constructed from the corresponding Jost function $f_\ell(k)$. The small-k behaviour of f_ℓ determines the threshold structure of the resolvent.

To first Born order, the correction to the Jost function contains

$$\int_0^\infty r^2 V(r) j_\ell(kr)^2\, dr = \int_0^\infty \frac{C}{r}\, j_\ell(kr)^2\, dr + (\text{short-range terms}), \tag{14}$$

where j_ℓ denotes the spherical Bessel function. The non-analytic contribution arises from the large-r region of this integral, where the potential behaves as C/r^3. Using the oscillatory asymptotics

$$j_\ell(kr) \sim \frac{\sin(kr - \ell\pi/2)}{kr}, \qquad r \to \infty, \tag{15}$$

one finds that the large-r contribution behaves schematically as

$$\int^{\infty} \frac{1}{r}\, e^{2ikr}\, dr \;\sim\; \log k, \qquad k \to 0. \tag{16}$$

Thus the critical r^{-3} tail produces a logarithmic non-analyticity at threshold. Standard results in low-energy scattering theory for borderline long-range potentials imply the expansion

$$f_\ell(k) = \sum_{j=0}^{2\ell+1} a_j k^j + b_\ell\, k^{2\ell+2} \log k + O(k^{2\ell+2}), \qquad k \to 0, \tag{17}$$

where the coefficients a_j depend on the full potential, while b_ℓ depends only on the coefficient C of the r^{-3} tail. In particular, b_ℓ vanishes if and only if the r^{-3} term is absent. The logarithmic term therefore reflects the asymptotic curvature decay and is insensitive to the detailed near-field geometry.

Since the Green function in each channel is constructed from $f_\ell(k)$, the logarithmic term produces a branch point at $k = 0$ in the frequency-domain resolvent.

From branch cut to late-time power law. The retarded field may be obtained by deforming the inverse Fourier contour onto the branch cut along $\omega \geq 0$. The discontinuity across the cut is controlled by the coefficient of the non-analytic term. A standard Tauberian argument then yields

$$h_\ell(t, x) \sim A_\ell(x)\, t^{-(2\ell+3)}, \qquad t \to \infty, \tag{18}$$

where the amplitude A_ℓ depends on the source, the observation point, and the asymptotic mass parameter through C.

For the lowest radiative gravitational multipole $\ell = 2$, this gives

$$h_2(t, x) \sim t^{-7}, \tag{19}$$

which coincides with Price's law for spin-2 perturbations on Schwarzschild. The exponent $2\ell + 3$ is therefore determined solely by the critical r^{-3} curvature decay and is not tied to the detailed structure of the Schwarzschild potential.

Universality and the role of the ADM mass. Let (Σ, g) be an asymptotically flat vacuum initial data set with ADM mass $M \neq 0$. The asymptotic expansion of the metric implies

$$|\mathrm{Riem}(x)| \sim C_M r^{-3}, \qquad r \to \infty, \tag{20}$$

with C_M proportional to M. Generically, this produces a nonvanishing r^{-3} term in the effective potential of the linearized operator in each angular momentum channel. Consequently:

$$M \neq 0 \implies |\mathrm{Riem}| \sim r^{-3} \implies \text{threshold non-analyticity} \implies t^{-(2\ell+3)} \text{ decay.} \tag{21}$$

If $M = 0$, the r^{-3} curvature term is absent, the threshold logarithm does not appear, and the resolvent is analytic at $\omega = 0$. In that case the retarded solution obeys Huygens' principle in $3 + 1$ dimensions and no power-law tail occurs. The onset of late-time tails is therefore tied to the presence of nonzero ADM mass.

Centrifugal hierarchy and scalar contrast. The angular momentum barrier suppresses the strength of the non-analytic term in higher channels. For $\ell = 0$ (relevant to scalar perturbations), the logarithmic term appears at order $k^2 \log k$, yielding the well-known t^{-3} decay. For $\ell = 2$, the first non-analytic contribution occurs at order $k^6 \log k$, leading to t^{-7}. The exponent is fixed by the threshold expansion, while the amplitude reflects both the asymptotic mass and the centrifugal barrier.

Testable prediction. Consider a stationary, asymptotically flat vacuum spacetime lacking exact spherical symmetry, for example a static solution constructed via Corvino-Schoen gluing. Provided the ADM mass is nonzero, the asymptotic curvature decay remains r^{-3}. The present analysis predicts that linearized perturbations on such a background exhibit the same $t^{-(2\ell+3)}$ late-time exponents as on Schwarzschild. The exponent should therefore be governed by the asymptotic curvature decay rather than by detailed near-field geometry.

Extension to Kerr spacetimes. The argument extends to Kerr backgrounds. Although the Teukolsky separation introduces frequency-dependent angular eigenvalues and coupling between spin-weighted modes, these effects are analytic in ω near $\omega = 0$. In particular, the spin–weighted spheroidal harmonics reduce to the corresponding spherical harmonics at zero frequency, and the angular eigenvalues admit analytic expansions in ω in a neighbourhood of $\omega = 0$.

The radial Teukolsky equation has an effective potential whose large-r asymptotics take the form

$$V(r) = \frac{\ell(\ell+1)}{r^2} + \frac{C_{a,m}}{r^3} + O(r^{-4}), \qquad r \to \infty, \tag{22}$$

where the centrifugal term $\ell(\ell+1)/r^2$ coincides with the Schwarzschild case, while the coefficient $C_{a,m}$ of the r^{-3} term depends on the spin parameter a and azimuthal number m but not on the decay exponent. The critical r^{-3} behaviour is therefore unchanged by rotation.

Consequently, the Jost function in each mode acquires the same $k^{2\ell+2}\log k$ threshold structure, and the outgoing resolvent possesses a branch point at $k = 0$ for all values of a. The late–time tail therefore satisfies

$$h_\ell(t, x) \sim t^{-(2\ell+3)}, \qquad t \to \infty, \tag{23}$$

with an exponent independent of the black hole spin. This agrees with the analytic and numerical results of Barack and Ori, who showed that late-time tails on Kerr decay with the same power law as on Schwarzschild.

The present paper works on time-symmetric slices. For Kerr initial data the extrinsic curvature contributes additional r^{-3} terms to the spatial constraint operator; however, the decay exponent of the asymptotic curvature remains r^{-3}, and therefore the threshold structure and the resulting tail exponent are unchanged. Within the present framework, the geometric reason is that the decay exponent is controlled by the asymptotic curvature rate $|\mathrm{Riem}| \sim r^{-3}$, which is determined by the ADM mass and is insensitive to the angular momentum of the source.

7 Relation to Threshold Phenomena and Infrared Structure

The inverse-cube decay identified in this work connects several strands of spectral theory, gravitational physics, and infrared field theory. While threshold phenomena for long-range operators have been studied extensively in other settings, the present result isolates a geometric mechanism specific to curvature-coupled tensor operators on asymptotically flat manifolds.

Connection with Schrödinger threshold theory

In three spatial dimensions, Schrödinger operators with potentials decaying as r^{-3} occupy a critical position between short- and long-range behavior. Faster decay yields purely absolutely continuous spectrum with uniform resolvent bounds at zero energy, while slower decay permits threshold obstructions and long-range scattering effects.

The spatial Lichnerowicz operator exhibits an analogous structure. The curvature term acts as an effective potential whose inverse-cube decay marks the boundary between spectrally negligible and marginal behavior. At this rate, zero enters the essential spectrum and the weighted resolvent develops a threshold singularity. In this sense, the gravitational case realizes, at the tensorial level, the same critical scaling that governs scalar long-range potentials.

Relation to late-time tails. The connection between the threshold resolvent singularity and late-time power-law decay has been established in Section 6.6. In particular, the $t^{-(2\ell+3)}$ tails arise directly from the logarithmic branch point of the outgoing resolvent at $\omega = 0$ induced by the critical r^{-3} curvature decay. We therefore do not repeat that analysis here.

Infrared structure and asymptotic symmetries

Much of the modern understanding of gravitational infrared physics has been formulated in terms of asymptotic symmetries at null infinity, soft graviton theorems, and memory effects. In that framework, the soft sector arises from the structure of radiative data and associated conservation laws.

The perspective adopted here is complementary. Rather than beginning with null infinity or scattering amplitudes, we identify the infrared sector

directly in the spectral properties of the spatial Lichnerowicz operator. The breakdown of threshold resolvent regularity provides a geometric origin for the persistence of low-frequency correlations. The spatial operator already encodes the obstruction that later manifests dynamically as soft enhancement and memory.

This reframing does not replace asymptotic symmetry analyses; rather, it identifies the geometric condition under which such infrared phenomena must occur.

Parallel with non-Abelian gauge fields

A closely related threshold arises in non-Abelian gauge theory. The covariant Laplacian acting on adjoint fields contains curvature through $\mathrm{ad}(F_A)$, and inverse-cube decay of the field strength similarly marks the onset of long-range spectral behavior.

The shared scaling reflects dimensional balance rather than detailed dynamics. In both spin-1 and spin-2 theories, curvature decaying as r^{-3} in three spatial dimensions is precisely marginal with respect to dispersion. The infrared sector therefore has a universal geometric origin across gauge and gravitational settings.

Summary of the structural picture

Taken together, these connections suggest that the inverse-cube decay is not an isolated curiosity but a universal spectral boundary. For $p > 3$, curvature is spectrally short-range and the theory remains radiative. At $p = 3$, a threshold singularity appears and the infrared sector emerges continuously. For $p < 3$, curvature becomes genuinely long-range and enhances low-energy coupling further.

The present work identifies this boundary explicitly for the spatial Lichnerowicz operator and quantifies the associated resolvent growth at threshold. In doing so, it links geometric decay, spectral structure, and gravitational infrared physics within a single framework.

8 Conclusion

This work identifies a geometric threshold governing the infrared structure of linearized gravity on asymptotically flat spatial slices. In three spatial dimensions, curvature decaying as $|\mathrm{Riem}(x)| \sim r^{-3}$ marks the precise boundary at which dispersion and curvature balance.

At this inverse-cube decay rate, zero enters the essential spectrum of the spatial Lichnerowicz operator and the weighted resolvent develops a quantitative threshold singularity,

$$\|\langle r\rangle^{-s}(L - i\varepsilon)^{-1}\langle r\rangle^{-s}\| \gtrsim \varepsilon^{-(1-s)}.$$

The limiting absorption principle therefore fails at zero energy. This breakdown of threshold resolvent regularity provides a spatial mechanism underlying the gravitational infrared sector.

The same geometric condition explains the persistence of large-distance correlations, the irregularity of low-frequency scattering, the emergence of soft gravitons, and the appearance of late-time power-law tails. These phenomena are not separate effects but different manifestations of a single resolvent singularity. In particular, the late-time power-law relaxation of perturbations follows from the branch cut structure of the resolvent at zero frequency, with the tail exponent $t^{-(2\ell+3)}$ determined by angular momentum channel and spatial dimension alone.

More generally, in d spatial dimensions the critical decay rate $|\mathrm{Riem}(x)| \sim r^{-d}$ marks the onset of infrared sensitivity for curvature-coupled Laplace-type operators. The inverse-cube decay in three dimensions is thus a special case of a universal dimensional balance.

By locating the origin of the soft sector in the spectral structure of the spatial Lichnerowicz operator, this work reframes gravitational infrared physics as a problem in geometric decay and threshold analysis. The infrared structure of gravity is already encoded on a Cauchy slice, prior to any reference to null infinity or scattering amplitudes.

A Gauge Correction and Elliptic Estimates

This appendix justifies the harmonic–gauge correction used in Section 3. Under the hypotheses of Section 5, namely, (Σ, g) smooth, asymptotically

flat, simply connected, and with $\mathrm{Ric} = O(r^{-3})$, the vector Laplacian

$$\Delta_V X = \nabla^* \nabla X + \mathrm{Ric}(X)$$

is uniformly elliptic and symmetric on $L^2(\Sigma; T^*\Sigma)$.

Lemma 1 (Isomorphism property)**.** *For weights $-1 < \delta < 0$, the mapping*

$$\Delta_V : H^2_\delta(\Sigma; T^*\Sigma) \to L^2_{\delta-2}(\Sigma; T^*\Sigma)$$

is Fredholm of index zero and an isomorphism whenever $H^1_{\mathrm{dR}}(\Sigma) = 0$.

Sketch. A direct consequence of Lockhart-McOwen theory (*Comm. Pure Appl. Math.* **38**, 603 (1985)), since the Euclidean indicial roots are $\{0, -2\}$. □

Lemma 2 (Gauge correction)**.** *For each $h \in H^2_\delta(\Sigma; S^2T^*\Sigma)$ with $-1 < \delta < 0$, there exists a unique $X \in H^2_\delta(\Sigma; T^*\Sigma)$ satisfying $\Delta_V X = \nabla \cdot h$ and $\|X\|_{H^2_\delta} \leq C\|\nabla \cdot h\|_{L^2_{\delta-2}}$.*

Proposition 1 (Corrected Weyl sequence)**.** *Let $\{h_n\}$ be the approximate sequence of Section 3. Defining $\tilde{h}_n = h_n - \mathcal{L}_{X_n} g$ with $X_n = \Delta_V^{-1}(\nabla \cdot h_n)$ yields*

$$\|\tilde{h}_n\|_{L^2} = 1, \qquad \tilde{h}_n \rightharpoonup 0, \qquad \|L\tilde{h}_n\|_{L^2} \to 0.$$

Thus $0 \in \sigma_{\mathrm{ess}}(L)$ in harmonic gauge.

B Curvature Structure and the Schwarzschild Example

The Schwarzschild metric provides a physical realization of the critical inverse–cube curvature decay analyzed in Section 3.

Definition 1 (Spatial metric)**.** *In isotropic coordinates (t, r, ω), the Schwarzschild line element is*

$$ds^2 = -\Big(\frac{1 - \frac{M}{2r}}{1 + \frac{M}{2r}}\Big)^2 dt^2 + \Big(1 + \frac{M}{2r}\Big)^4 (dr^2 + r^2 d\omega^2).$$

On a time-symmetric slice $t = \text{const.}$, the spatial metric is $g_{ij} = \psi^4 \delta_{ij}$ with $\psi(r) = 1 + \frac{M}{2r}$.

Lemma 3 (Asymptotic curvature)**.** *For this metric,*

$$|\mathrm{Riem}(x)| \simeq C\, M\, r^{-3} \qquad (r \to \infty),$$

so the curvature saturates the inverse–cube decay assumed in Theorem 2.

Proposition 2 (Effective potential)**.** *The spatial Lichnerowicz operator on the Schwarzschild background satisfies*

$$Lh = \Delta_0 h - (CM) r^{-3} h + O(r^{-4}) h, \qquad CM > 0,$$

showing that the Schwarzschild geometry realizes, in its far-field limit, the same attractive r^{-3} potential analyzed in the numerical model of Section 5. [1]

C Analytical Framework and Weighted Sobolev Spaces

We summarize the analytic conventions and functional-analytic tools used throughout.

Definition 2 (Weighted Sobolev spaces)**.** *For a smooth radius function r on an asymptotically flat three–manifold (Σ, g) and $\delta \in \mathbb{R}$,*

$$\|u\|^2_{H^k_\delta} = \sum_{|\alpha| \le k} \int_\Sigma (1 + r^2)^{\delta - |\alpha|} |\nabla^\alpha u|^2 \, dV_g.$$

Then $H^k_\delta(\Sigma; E)$ is the completion of $C^\infty_c(\Sigma; E)$ under this norm.

Lemma 4 (Fredholm property)**.** *If P is a uniformly elliptic operator approaching constant coefficients at infinity, then*

$$P : H^2_\delta \to L^2_{\delta - 2}$$

is Fredholm for all δ not equal to an indicial root [20].

Proposition 3 (Self-adjointness and essential spectrum)**.** *For $\delta \in (-1, 0)$ and $V = O(r^{-p})$ with $p > 2$, operators of the form $L = \nabla^*\nabla + V$ are self–adjoint on $L^2(\Sigma; E)$. The essential spectrum $\sigma_{\mathrm{ess}}(L)$ is determined by the existence of Weyl sequences as in Weyl's criterion.*

[1] The overall minus sign arises from the definition $(V_R h)_{ij} = -R_i{}^k{}_j{}^\ell h_{k\ell}$, which makes the curvature coupling attractive for positive mass $M > 0$.

Lemma 5 (Compactness of the curvature potential for $p > 3$)**.** *Let (Σ, g) be a smooth asymptotically flat three-manifold with a single Euclidean end, and assume*

$$g_{ij} = \delta_{ij} + O(r^{-1}), \qquad \partial g_{ij} = O(r^{-2}), \qquad \partial^2 g_{ij} = O(r^{-3}),$$

so that $|\mathrm{Riem}(x)| \leq C \langle r \rangle^{-p}$ for some $p > 3$. Fix a weight $-1 < \delta < 0$, and let

$$L = \nabla^* \nabla + V_R, \qquad (V_R h)_{ij} = -R_i{}^{\ell}{}_j{}^{m}\, h_{\ell m}.$$

Then the curvature term defines a compact operator

$$V_R : H^2_\delta(\Sigma; S^2 T^*\Sigma) \longrightarrow L^2_{\delta-2}(\Sigma; S^2 T^*\Sigma),$$

and therefore L is a compact perturbation of $\nabla^*\nabla$ on $L^2(\Sigma; S^2 T^*\Sigma)$. In particular,

$$\sigma_{\mathrm{ess}}(L) = \sigma_{\mathrm{ess}}(\nabla^*\nabla) = [0, \infty).$$

Proof. The curvature bound $|\mathrm{Riem}(x)| \leq C\langle r\rangle^{-p}$ implies $|V_R(x)| \leq C\langle r\rangle^{-p}$, so that for any $h \in H^2_\delta(\Sigma; S^2 T^*\Sigma)$,

$$\|V_R h\|^2_{L^2_{\delta-2}} = \int_\Sigma \langle r\rangle^{2(\delta-2)} \, |V_R(x) h(x)|^2 \, dV_g \lesssim \int_\Sigma \langle r\rangle^{2(\delta-2)-2p} |h(x)|^2 \, dV_g.$$

Since $-1 < \delta < 0$ and $p > 3$, the exponent $2(\delta - 2) - 2p$ is less than -6, making the weight $\langle r\rangle^{2(\delta-2)-2p}$ integrable at infinity in three dimensions. Hence $V_R : H^2_\delta \to L^2_{\delta-2}$ is bounded.

To verify compactness, let χ_R be a smooth cutoff equal to 1 on $\{r \leq R\}$ and supported in $\{r \leq 2R\}$. Decompose

$$V_R = \chi_R V_R + (1 - \chi_R) V_R =: V_R^{(\mathrm{comp})} + V_R^{(\mathrm{tail})}.$$

On the bounded region $\{r \leq 2R\}$, the metric is smooth and the weighted norms are equivalent to the unweighted ones. By the classical Rellich compactness theorem on precompact domains, the embedding $H^2_\delta(\{r \leq 2R\}) \hookrightarrow L^2_{\delta-2}(\{r \leq 2R\})$ is compact; since V_R is smooth there, the multiplication operator $V_R^{(\mathrm{comp})}$ is compact.

The remainder $V_R^{(\mathrm{tail})}$ is supported in $\{r > R\}$, where the curvature decay dominates. For h with $\|h\|_{H^2_\delta} = 1$,

$$\|V_R^{(\mathrm{tail})} h\|^2_{L^2_{\delta-2}} \lesssim \int_{r>R} \langle r\rangle^{2(\delta-2)-2p} |h(x)|^2 \, dV_g.$$

Because $2(\delta-2)-2p<-6$, the weight decays faster than r^{-6}; combined with the uniform bound $|h|^2 \in L^2_\delta$, dominated convergence implies that

$$\sup_{\|h\|_{H^2_\delta}=1} \|V_R^{(\mathrm{tail})} h\|_{L^2_{\delta-2}} \longrightarrow 0 \quad \text{as } R \to \infty.$$

Thus V_R is the limit of compact operators with vanishing tails, and hence compact.

Finally, since $L = \nabla^*\nabla + V_R$ is a compact perturbation of the nonnegative, self-adjoint operator $\nabla^*\nabla$, Weyl's theorem ensures that the essential spectra coincide:

$$\sigma_{\mathrm{ess}}(L) = \sigma_{\mathrm{ess}}(\nabla^*\nabla) = [0, \infty).$$

The essential spectrum of the Lichnerowicz operator therefore matches that of the flat tensor Laplacian, confirming that sufficiently rapid curvature decay leaves the asymptotic spectrum purely continuous. □

Remark 1. *These weighted spaces and mapping properties justify the estimates and compactness arguments used in Sections 2–3.*

D Numerical Validation and Stability

This appendix documents the discretization scheme, constraint enforcement, and convergence tests underlying the numerical results reported in Section 5. The purpose of this appendix is to verify that the observed spectral behavior is not an artifact of discretization, finite volume, or constraint implementation.

D.1 Discretization of the Spatial Operator

The spatial Lichnerowicz operator

$$L = \nabla^*\nabla + V_R$$

is discretized on a cubic domain

$$\Omega = [-R_{\max}, R_{\max}]^3$$

using a uniform Cartesian grid with spacing h. Second–order centered finite differences approximate ∇ and $\nabla^*\nabla$. The curvature potential V_R is evaluated pointwise from its asymptotic form C/r^p.

Dirichlet boundary conditions $h|_{\partial\Omega} = 0$ define a finite–volume eigenvalue problem. For the flat operator ($C = 0$), the lowest eigenvalue satisfies

$$\lambda_1^{\text{flat}}(R_{\max}) \sim \pi^2 R_{\max}^{-2},$$

reflecting the discretization of the continuum threshold by box modes. The observed scaling in the flat case confirms that the discretization reproduces the expected finite–volume behavior of the Laplacian.

The resulting discrete operator has the matrix form

$$L_h = K + V,$$

where K is the stiffness matrix associated with the finite–difference Laplacian and V is the diagonal matrix of curvature values.

All computations use double precision arithmetic. The lowest eigenvalues are obtained via a conjugate–gradient Lanczos solver with relative residual tolerance 10^{-5}.

D.2 Transverse–Traceless Constraint Enforcement

To restrict to transverse–traceless (TT) tensor fields, we employ a penalty formulation. The discrete Rayleigh functional is

$$\mathcal{R}_{\eta,\zeta}[h] = \frac{\langle h, L_h h\rangle + \eta \,\|\nabla\cdot h\|^2_{L^2(\Omega)} + \zeta \,\|\operatorname{tr} h\|^2_{L^2(\Omega)}}{\|h\|^2_{L^2(\Omega)}},$$

where $\eta, \zeta > 0$ are penalty parameters, $\nabla\cdot h$ is the discrete divergence, and $\operatorname{tr} h$ is the discrete trace.

Stationary points satisfy the generalized eigenvalue problem

$$(K + \eta D^\top D + \zeta T^\top T)u = \lambda M u,$$

where D and T denote the discrete divergence and trace operators, and M is the mass matrix.

To verify that the lowest eigenvalues correspond to the TT subspace, we perform parameter sweeps with η, ζ varied by factors of two to four. The resulting variation in λ_1 is less than 10^{-3} across all runs.

In addition, we explicitly project selected eigenmodes onto the TT subspace using the discrete Helmholtz decomposition. The L^2 norm difference between penalized and projected modes is below 10^{-3}, confirming that the penalty method faithfully enforces the constraint at the level of the lowest modes.

D.3 Grid Refinement and Resolution Study

To assess discretization error, we compute λ_1 for grid spacings $h \in \{1.0,\, 0.75,\, 0.5\}$ at fixed $R_{\max}$.

The dependence of $\lambda_1(h)$ is well approximated by

$$\lambda_1(h) = \lambda_1 + Ch^2 + O(h^3),$$

consistent with second–order convergence. The change in λ_1 between $h = 0.75$ and $h = 0.5$ is below 2% in all cases reported in Section 5. Extrapolation to $h \to 0$ does not alter the qualitative dependence of λ_1 on p or $R_{\max}$.

These tests confirm that the spectral trends are not resolution artifacts.

D.4 Finite–Volume Scaling and Box–Mode Interpretation

For $p \geq 3$, the lowest eigenvalue satisfies

$$\lambda_1(R_{\max}) \sim R_{\max}^{-2},$$

mirroring the flat–space scaling. To quantify this behavior, we perform least–squares fits of the form

$$\lambda_1(R_{\max}) = aR_{\max}^{-2} + bR_{\max}^{-3}.$$

The residuals are below 5% across the range $R_{\max} \in \{6, 10, 14, 18, 20\}$, indicating that the leading scaling is governed by finite–volume discretization of the continuum edge.

For $p < 3$, the same fitting procedure reveals systematic downward shifts in a, reflecting enhanced infrared coupling, but no negative eigenvalues appear. This confirms that the transition at $p = 3$ is continuous and does not produce discrete bound states.

D.5 Radial Model Consistency

The Rayleigh–quotient diagnostic employs the asymptotic radial model

$$L_p = -\frac{d^2}{dr^2} + \frac{\ell(\ell+1)}{r^2} + \frac{C}{r^p}.$$

Projection of the full tensor operator onto angular harmonics produces an effective radial potential of this form, with subleading corrections $O(r^{-p-1})$. The measured scaling

$$\Delta E(R,p) \sim R^{-(p-2)}$$

is insensitive to the choice of angular mode ℓ, confirming that the diagnostic captures the asymptotic channel structure of the full operator.

Taken together, the discretization tests, penalty sweeps, grid refinement studies, and finite–volume scaling analysis demonstrate that the numerical results reported in Section 5 faithfully represent the spectral behavior of the spatial Lichnerowicz operator and are not artifacts of discretization or constraint implementation.

E Weyl Sequence Construction and Threshold Resolvent Estimate

This appendix provides the detailed construction of the Weyl sequence used in Section 3 and the full estimate chain leading to the threshold resolvent growth bound in the three–dimensional critical case $|\mathrm{Riem}(x)| \sim r^{-3}$.

Throughout, (Σ, g) is an asymptotically flat three–dimensional Riemannian manifold, and the spatial Lichnerowicz operator acting on symmetric two–tensors is

$$L = \nabla^*\nabla + V_R.$$

All constructions below are carried out in $d = 3$.

E.1 Construction of Annular Tensor Fields

Let $\chi \in C_c^\infty([1,2])$ be a nontrivial smooth cutoff. For each integer $n \geq 1$, define

$$\chi_n(r) = \chi\Big(\frac{r}{n}\Big), \qquad \mathrm{supp}(\chi_n) \subset \{r \in [n, 2n]\}.$$

Let $T_{ij}(\omega)$ be a fixed smooth symmetric transverse–traceless tensor field on S^2, chosen to be a tensor harmonic of order $\ell = 2$. Define the preliminary fields

$$h_n(x) = \chi_n(r)\, r^{-1/2} T_{ij}(\omega), \qquad \omega = x/r.$$

The factor $r^{-1/2}$ is forced by asymptotic flatness and finite L^2 energy on three–dimensional spatial slices. Indeed,

$$\int_n^{2n} r^2 \cdot r^{-1}\, dr = \int_n^{2n} r\, dr \sim n^2,$$

so $\|h_n\|_{L^2} \sim n$. After normalization,

$$\hat{h}_n = \frac{h_n}{\|h_n\|_{L^2}}, \qquad \|\hat{h}_n\|_{L^2} = 1.$$

The fields h_n are traceless but not exactly divergence–free, since differentiation of the cutoff produces

$$\nabla \cdot h_n = O(n^{-1}) r^{-1/2}$$

on their support.

E.2 Gauge Correction to Exact Transversality

To enforce the transverse condition, we solve the vector Poisson equation

$$\Delta_V X_n = \nabla \cdot \hat{h}_n,$$

where Δ_V is the vector Laplacian. Standard elliptic estimates on asymptotically flat manifolds yield

$$\|X_n\|_{H^2} \lesssim \|\nabla \cdot \hat{h}_n\|_{L^2}.$$

Since $\nabla \cdot \hat{h}_n = O(n^{-1})$ in L^2, it follows that

$$\|X_n\|_{H^2} \lesssim n^{-1}.$$

Define the corrected fields

$$\tilde{h}_n = \hat{h}_n - \mathcal{L}_{X_n} g,$$

where $\mathcal{L}_{X_n} g$ denotes the Lie derivative of the metric.

By construction,

$$\nabla \cdot \tilde{h}_n = 0, \qquad \text{tr } \tilde{h}_n = 0.$$

Moreover,

$$\|\mathcal{L}_{X_n} g\|_{L^2} \lesssim \|X_n\|_{H^1} \lesssim n^{-1}.$$

Thus

$$\|\tilde{h}_n - \hat{h}_n\|_{L^2} \lesssim n^{-1},$$

so normalization is preserved up to $O(n^{-1})$ corrections, and we may renormalize so that

$$\|\tilde{h}_n\|_{L^2} = 1.$$

E.3 Residual Estimate

We estimate $\|L\tilde{h}_n\|_{L^2}$.

First consider h_n. On flat space, the Laplacian annihilates $r^{-1/2}T_{ij}(\omega)$ for tensor harmonics of order $\ell = 2$. Therefore, in the asymptotic region, the only contributions to $\nabla^*\nabla h_n$ arise from:

(i) commutators $[\nabla^*\nabla, \chi_n]$, and (ii) curvature corrections to the connection.

The commutator term yields

$$[\nabla^*\nabla, \chi_n](r^{-1/2}T) = O(n^{-2})$$

in L^2, since $\partial_r\chi_n = n^{-1}\chi'(r/n)$ and second derivatives scale as n^{-2}.

The curvature term satisfies

$$V_R h_n = O(r^{-3})h_n,$$

so on the support $r \sim n$,

$$\|V_R h_n\|_{L^2} \lesssim n^{-3}.$$

Combining these contributions,

$$\|Lh_n\|_{L^2} \lesssim n^{-2}\|h_n\|_{L^2}.$$

After normalization and gauge correction,

$$\boxed{\|L\tilde{h}_n\|_{L^2} \leq Cn^{-2}.}$$

The gauge correction contributes only subleading $O(n^{-2})$ terms and does not alter the scaling.

E.4 Weighted Norm Scaling

On the support of $\tilde{h}_n$,

$$\langle r \rangle \sim n.$$

Hence

$$\|\langle r \rangle^s \tilde{h}_n\|_{L^2} \sim n^s, \qquad \|\langle r \rangle^{-s} \tilde{h}_n\|_{L^2} \sim n^{-s}.$$

These relations follow from the fact that $\langle r \rangle^{\pm s}$ varies by at most a fixed factor on $[n, 2n]$.

E.5 Threshold Resolvent Growth Estimate

Let

$$T_\varepsilon = \langle r \rangle^{-s} (L - i\varepsilon)^{-1} \langle r \rangle^{-s}, \qquad s \in (1/2, 1).$$

Define

$$g_{n,\varepsilon} = \langle r \rangle^s (L - i\varepsilon) \tilde{h}_n.$$

Using the residual and weighted estimates,

$$\|g_{n,\varepsilon}\|_{L^2} \lesssim n^{s-2} + \varepsilon n^s.$$

Choosing $\varepsilon \sim n^{-2}$ gives

$$\|g_{n,\varepsilon}\|_{L^2} \lesssim n^{s-2}.$$

Since

$$T_\varepsilon g_{n,\varepsilon} = \langle r \rangle^{-s} \tilde{h}_n,$$

we obtain

$$\|T_\varepsilon\| \gtrsim \frac{n^{-s}}{n^{s-2}} = n^{2-2s}.$$

Substituting $n = \varepsilon^{-1/2}$ yields

$$\boxed{\|T_\varepsilon\| \gtrsim \varepsilon^{-(1-s)}.}$$

This establishes the quantitative threshold resolvent singularity used in Section 3.

Declarations

Funding The author received no external funding.

Conflict of interest The author declares no conflict of interest.

Data availability All data supporting the conclusions of this work are contained within the article and its Supplementary Material. No external datasets were used. Numerical results can be reproduced using the procedures described in Section 5 and Appendix D.

References

[1] Ya. B. Zel'dovich and A. G. Polnarev, "Radiation of gravitational waves by a cluster of superdense stars," Sov. Astron. **18**, 17-23 (1974).

[2] D. Christodoulou, "Nonlinear nature of gravitation and gravitational-wave experiments," Phys. Rev. Lett. **67**, 1486-1489 (1991).

[3] S. Weinberg, "Infrared photons and gravitons," Phys. Rev. **140**, B516-B524 (1965).

[4] A. Strominger, *Lectures on the Infrared Structure of Gravity and Gauge Theory* (Princeton University Press, Princeton, 2018).

[5] T. He, V. Lysov, P. Mitra, and A. Strominger, "BMS supertranslations and Weinberg's soft graviton theorem," JHEP **1505**, 151 (2015); arXiv:1401.7026.

[6] F. Cachazo and A. Strominger, "Evidence for a new soft graviton theorem," arXiv:1404.4091 (2014).

[7] L. Bieri and D. Garfinkle, "An electromagnetic analogue of gravitational wave memory," Class. Quantum Grav. **30**, 195009 (2013); arXiv:1307.5098.

[8] H. Bondi, M. G. J. van der Burg, and A. W. K. Metzner, "Gravitational waves in general relativity. VII. Waves from axisymmetric isolated systems," Proc. R. Soc. Lond. A **269**, 21-52 (1962).

[9] R. K. Sachs, "Gravitational waves in general relativity. VIII. Waves in asymptotically flat space-times," Proc. R. Soc. Lond. A **270**, 103-126 (1962).

[10] R. H. Price, "Nonspherical perturbations of relativistic gravitational collapse. I. Scalar and gravitational perturbations," Phys. Rev. D **5**, 2419-2438 (1972).

[11] E. S. C. Ching, P. T. Leung, W. M. Suen, and K. Young, "Late-time tail of wave propagation on curved spacetime," Phys. Rev. Lett. **74**, 4588-4590 (1995).

[12] M. Dafermos and I. Rodnianski, "A proof of Price's law for the collapse of a self-gravitating scalar field," Invent. Math. **162**, 381-457 (2005); arXiv:gr-qc/0309115.

[13] T. Regge and J. A. Wheeler, "Stability of a Schwarzschild singularity," Phys. Rev. **108**, 1063-1069 (1957).

[14] S. Chandrasekhar, *The Mathematical Theory of Black Holes* (Oxford University Press, Oxford, 1983).

[15] B. Simon, "On the genericity of nonvanishing of the low energy spectral density for Schrödinger operators," Ann. Phys. (N.Y.) **97**, 279-288 (1976).

[16] A. Jensen and T. Kato, "Spectral properties of Schrödinger operators and time-decay of the wave functions," Duke Math. J. **46**, 583-611 (1979).

[17] E. Mourre, "Absence of singular continuous spectrum for certain self-adjoint operators," Comm. Math. Phys. **78**, 391-408 (1981).

[18] D. R. Yafaev, *Mathematical Scattering Theory: Analytic Theory*, Mathematical Surveys and Monographs, Vol. 158 (American Mathematical Society, Providence, 2010).

[19] M. Reed and B. Simon, *Methods of Modern Mathematical Physics, Vol. IV: Analysis of Operators* (Academic Press, New York, 1978).

[20] R. B. Lockhart and R. C. McOwen, "Elliptic differential operators on noncompact manifolds," Ann. Scuola Norm. Sup. Pisa Cl. Sci. (4) **12**, 409-447 (1985).

[21] R. B. Lockhart and R. C. McOwen, "On elliptic systems in $\mathbb{R}^n$," Acta Math. **150**, 125-135 (1983).

[22] R. Bartnik, "The mass of an asymptotically flat manifold," Comm. Pure Appl. Math. **39**, 661-693 (1986).

[23] S. Agmon, *Lectures on Exponential Decay of Solutions of Second-Order Elliptic Equations* (Princeton University Press, Princeton, 1982).

[24] P. R. Chernoff, "Essential self-adjointness of powers of generators of hyperbolic equations," J. Funct. Anal. **12**, 401-414 (1973).

[25] N. D. Birrell and P. C. W. Davies, *Quantum Fields in Curved Space* (Cambridge University Press, Cambridge, 1982).

[26] R. M. Wald, *Quantum Field Theory in Curved Spacetime and Black Hole Thermodynamics* (University of Chicago Press, Chicago, 1994).

[27] A. Ashtekar and M. Streubel, "Symplectic geometry of radiative modes and conserved quantities at null infinity," Proc. R. Soc. Lond. A **376**, 585-607 (1981).

[28] M. Wilson, "Curvature decay and the spectrum of the non-Abelian Laplacian on $\mathbb{R}^3$," arXiv:2511.03532 (2025); submitted to J. Spectral Theory.

[29] H. Weyl, "Über gewöhnliche Differentialgleichungen mit Singularitäten und die zugehörigen Entwicklungen willkürlicher Funktionen," Math. Ann. **68**, 220-269 (1910).